

FUNCTIONAL AERODYNAMICS AND ITS INFLUENCE ON THE ENERGY AND THERMAL MODE OF A NATURALLY VENTILATED DOUBLE-SKIN TRANSPARENT FAÇADE

MICHAL FRANEK^{a,*}, BORIS BIELEK^a, MAREK MACÁK^b, JOSIP KLEM^a

^a Slovak University of Technology in Bratislava, Faculty of Civil Engineering, Department of Building Structures, Radlinského 2766/11, 810 05 Bratislava, Slovakia

^b Slovak University of Technology in Bratislava, Faculty of Civil Engineering, Department of Mathematics and Descriptive Geometry, Radlinského 2766/11, 810 05 Bratislava, Slovakia

* corresponding author: michal.franek@stuba.sk

ABSTRACT. This article deals with the dynamics of airflow through a cavity. In windless conditions, where a natural flow causes the flow of air in the cavity, the overall aerodynamic resistance of the cavity is the important aerodynamic parameter, which is the sum of the local resistances alongside the air movement trajectory through the cavity. The total aerodynamic resistance of the cavity must be less than the force of the convective buoyancy of the air in the cavity. The following conclusions were found experimentally. The convection occurs in the cavity at every time step with a velocity range from $0.05 \leq v$ [m/s] ≤ 0.2 to 0.3. The energy regime in the cavity is characterised by inhomogeneity. In the cavity, there are zones of increasing temperatures along the height of the cavity at the inlet. A large area with increased temperatures at the air outlet and a small area with particularly high temperatures in the upper part of the inlet were found.

KEYWORDS: double-skin transparent façade, energy and thermal mode, aerodynamic resistance of the cavity, total pressure coefficient.

1. LIST OF ACRONYMS

BLWT	Boundary Layer Wind Tunnel
CFD	Computational Fluid Dynamics
DNS	Direct Numerical Simulation
DSTF	Double-Skin Transparent Façade
LES	Large Eddy Simulation
N-S	Navier-Stokes
RANS	Reynolds Averaged Navier-Stokes Equations
SRS	Scale-Resolving Simulation
NBS	National Bank of Slovakia

2. INTRODUCTION

There are many factors that affect the technology of construction of façades, such as architectural trends, technology itself, and public requests. Today, the importance of environment specific contexts is as important as public requests for the quality of work. Current modern trends, such as ecology, energy-saving, automatic control systems, have not been addressed by façade technology, which also uses ecological renewable energy sources, which follow the concept of ecological improvement in the European construction industry.

One of the most environmentally friendly alternative sources of solar energy is the double-skinned transparent façade (DSTF), the concept of which is not new, but the trend of constructing buildings with DSTF has only recently been growing, mostly in Europe because of high energy costs and ecological awareness.

The originality in the creation of a new façade technology is characterised by four aspects:

- theory of the creation of new façade technology is designated for intelligent buildings,
- façade elements have the character of items of circuits of automated systems of building control,
- façade elements or systems have the ability to utilise natural physical phenomena,
- façade elements or systems have the ability to dynamically reduce the required volume of the environment technology of the building [1].

Considering the technical aspect, the development of a double-skin transparent façade has its foundations in the physical theory of cavities, which allows various adjustments, e.g., in the geometry of the cavity or in the type of glazing used. The theory of natural physical cavities has its roots in the development of recent technical disciplines, which are solar heat technology and aerodynamics of buildings with their substantial activity in the field of the physics of buildings and constructions. Cavity theory quantifies their physical behaviour, called multi-skin structures, and has been a topic discussed by many authors. There are many

ways to design DSTF and predict its behaviour, such as models for predicting the airflow or temperature inside a cavity. Underestimating the systems and components of the DSTF as a whole can result in major errors that significantly affect its operation. We can find proof of this in existing buildings, which have these problems [2], [3].

Todorovic et al. [2] developed a computational model usable in the climatic environment of Central Europe that approximates the temperature of the air and the heating (cooling) load in the DSTF cavity every hour. Arons [3] used a numerical model for a calculation of energy performance of a typical DSTF. In 2001, Gan [4] used a model for calculating the thermal transmittance of multiple glazing based on computational fluid dynamics (CFD), and in experimental cases, Saelens et al. [5] introduced a numerical model for calculating the thermal power of active envelopes. Later, Hensen et al. [6] used a network to calculate the characteristics of the air inside the DSTF cavity and included it in the thermal and energy model of the building. A model for single-storey buildings was presented by Saelens [7], he created a computational algorithm for two dimensional double-skin façades with both mechanical and natural ventilation. In Belgium, Gratia et al. [8] developed a model for thermal efficiency and cooling (heating) load according to the season. Grabe [9] developed a practice for modelling the temperature and air behaviour in DSTF. More modern works include computational fluid dynamics models, which can calculate airflow in DSTF cavity more accurately as compared to abovementioned models [10], [11], [12]. Manz et al. [13] used an algorithm to calculate the heat transfer from a natural convection in DSTF. The CFD method can offer much more detailed results especially for airflow through shading devices, recirculation zones or when the wind profile is irregular [13], [14], [15]. A brief document was issued in 2007 by the Commission of the European Council [16] with guiding principles for the construction of DSTF.

In the case of double-skin transparent façades using an alternative source of solar energy, the transformation of short-wave solar radiation into long-wave heat radiation is a natural physical phenomenon [17], [18]. The exploitation of this physical phenomenon with contribution of quantified dynamics of air flows is conditioned by the development of the theory of physical cavities.

The double-skin transparent façade participates in energy conservation of buildings in winter periods by its energy, which is gained from renewable energy sources – solar radiation and also by the transformation of solar radiation into heat radiation in the cavity of the façade. Well-designed aerodynamics of cavity can also meaningfully decrease the heat load of a building in summer seasons [19]. The double-skin transparent façade offers the possibility of natural ventilation, which is directly connected to the outside

climate. At the same time, it delivers a new quality of psycho-physiological comfort in the working space. It is characterised by a better connection of an artificial architectural environment with nature.

The main objective of this article is the new façade technology for buildings, that is the double-skin transparent façade in Figure 1.

The methodology of the paper is a theoretical analysis based on scientific disciplines and in-situ measurement:

- building solar thermal technology in a more complex perception, including the input of solar radiance,
- aerodynamics of buildings in „a more complex perception than that represented by a rigid model“ with an external pressure coefficient c_{pe} (-), quantified by an aerodynamic coefficient of overall pressure $c_p = c_{pe} - c_{pi}$ (-), in which the knowledge of the aerodynamic coefficient of internal pressure c_{pi} (-) substitutes for the imperfection of a rigid model,
- aerodynamics of a cavity, quantified by the overall aerodynamic resistance of the cavity Z , which is the sum of the friction resistances and local resistances lengthways to the flow trajectory in the cavity.

3. THEORETICAL BACKGROUND

The physical theory of cavities is the base idea of the double-skin transparent façade. The paper deals with a naturally ventilated double-skin transparent façade with a corridor-type cavity (cavity width $0.5 \leq b \leq 1.5$ m) and open circuit (the whole volume of air entering the cavity is air flowing from the outdoor climate, also, the entire volume of air through the cavity is conducted to the outdoor climate) in Figure 2.

A general correlation of the temperature in the cavity (Figure 2) is visible if the external air enters the cavity:

$$\theta_{a,OUTLET} - \theta_{a,INLET} = \theta_{a,OUTLET} - \theta_{ae} = \frac{\tau_g \cdot I_m}{mean U_m} (1 - e^{-\frac{mean U_m \cdot L}{q_m \cdot c} H}), \quad (1)$$

where $\theta_{a,OUTLET}$ is the air temperature from the outlet of the cavity [°C], $\theta_{a,INLET}$ is the air temperature from the inlet of the cavity [°C], τ_g is the overall transmission coefficient of the glazed system of the front – outer transparent wall [-], I_m is the mean intensity of global solar irradiation on the outer vertical transparent wall [W/m²], $mean U_m$ is the mean heat transfer coefficient of the bounding structures of the cavity [W/(m² · K)], L is the length (horizontal) of the cavity division [m], q_m is the mass air flow rate through the cavity [kg/s], H is the height of the cavity [m], c is the mass heat capacity of the air [J/(kg · K)]. The energy regime of these cavities depends on the air flow rate q_m [kg/s], q_v [m³/s], which is determined by the dynamics of the air flowing through the cavity

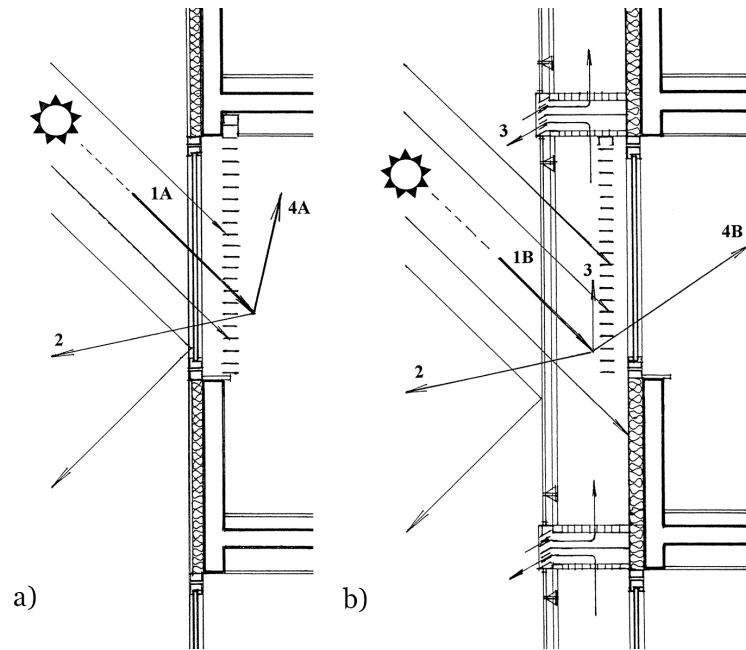


FIGURE 1. Illustration of classic transparent façade and double-skin transparent façade: a) classic transparent façade, b) double-skin transparent façade: 1A global solar radiation transmitted into the building, 1B – global solar radiation transmitted to the cavity, 2 – heat flux by transfer to the exterior, 3 – heat consumed to heat the air and conducted to the outside climate, 4A – heat load of the building in summer, 4B – heat flux through the transfer to the building – heat load of the building core during the summer.

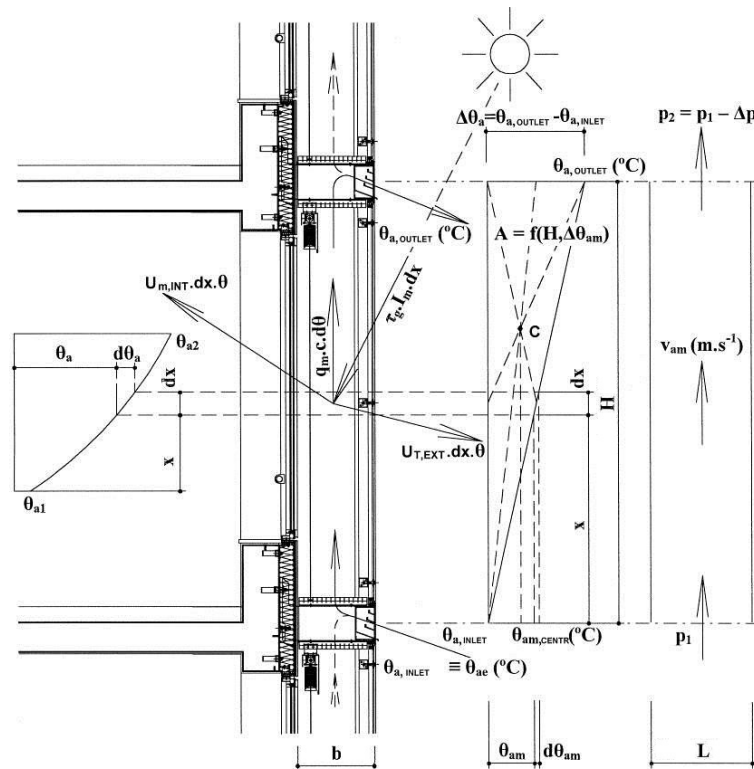


FIGURE 2. Quantification of aerodynamic and energy regimes of DSTF with open circuit. Width of cavity is $0.5 \leq b \leq 1.5$ m (corridor type cavity). Height of the cavity H [m] is identical to floor height.

based on natural convection, wind, and their combination.

3.1. AERODYNAMIC QUANTIFICATION OF THE CAVITY

It is necessary to know the total aerodynamic resistance of the cavity for the quantification of the air flow rate q_m [kg/s] under the windless conditions:

$$Z = 1 + \sum Z_l + \sum Z_m = 1 + \sum \frac{\bar{\lambda} \cdot (H + b)}{D_h} + \sum_{x=1}^{10} \xi_x, \quad (2)$$

where $\sum Z_l$ is the sum of the frictional resistance along the entire height of the cavity [-], $\sum Z_m$ is the sum of the local aerodynamic resistance [-], H is the cavity height [m], b is the cavity width [m], $\bar{\lambda}$ is the coefficient of the friction along the entire height of the cavity [-], $\bar{\lambda} = f(Re)$, Re [-] is Reynolds number, as mentioned in Figure 3, ξ_x is the aerodynamic coefficients of local resistance along the airflow trajectory through the cavity [-] as explained in Figure 4, D_h is the aerodynamic cavity diameter [m].

The resistances are longitudinally directly proportional to the length of the trajectory of the movement of the airflow in the cavity $H + b$ (Eq. 2), as shown in Figure 2, and which is in contrast to the diameter of the cavity D_h [m]. Local resistances are connected to the exact space of the airflow movement inside the cavity and are made of parts where the speed or path of the airflow differs (Fig. 2).

It is essential that the total aerodynamic resistance Z must be lesser than the convective air buoyancy power of the air in the cavity, if we want to achieve the required airflow through the cavity in all climatic situations (including the windless situation):

$$\max Z = 1 + \sum \frac{\bar{\lambda} \cdot (H + b)}{D_h} + \sum_{x=1}^n \xi_x < 18, \quad (3)$$

Two local resistances are vital in order to calculate Z (Eq. 3):

- (1.) the local aerodynamic resistance at the inlet of the channel ξ_1 with rain protective louvers A ξ_2 , which characterizes the turbulence at the outlet of the channel B (Fig. 4),
- (2.) the local aerodynamic resistance at the outlet channel from the cavity ξ_{10} with a rain louver A ξ_9 , which is responsible for the turbulence of the air flow from the output channel G (Fig. 4).

The rain louvers at the inlet and outlet have a role to prevent the penetration of rainwater from wind-driven rain into the cavity. The aerodynamic coefficients of the local resistances are determined in accordance with the aerodynamic theory shown in Figures 5 and 6.

The slats of louvres can be designed as classical rain screens or aerodynamic slats. Their local aerodynamic resistances at the inlet of a distribution channel are shown in Figure 7, and the outlet of the distribution channel is shown in Figure 8.

From the analysis of drag coefficients, conventional rain louvers on an inlet of DSTF are not optimal. It can be summarized as follows:

- (1.) The optimal ratio to the total area with conventional rain louvers cannot be ensured (Eq. 4):

$$\frac{a}{A} \cdot 100 \cong 80\%, \quad (4)$$

where a is a net area of openings for the air flow, and A is the total inlet area of the air, including the louvers.

- (2.) Typical rain louvers lead to a high local drag coefficient at the inlet (ξ_1), and especially at the outlet (ξ_{10}).

These facts affect the overall aerodynamic drag of the cavity to such a large extent, that it is not possible to ensure the requirement given by Eq. 5:

$$\text{opt.} Z = 1 + \sum \frac{\bar{\lambda} \cdot (H + b)}{D_h} + \sum_{x=1}^{n=10} \xi_x = 18, \quad (5)$$

The convective buoyancy of air is still higher than the overall aerodynamic resistance of the cavity Eq. 5. It means that the convective movement of the air flow is ensured in the cavity naturally without any wind. But the application of conventional louvers leads to the large drag coefficient, which blocks the naturally convective flow. Therefore, it is recommended to use the aerodynamic louvers with local resistances of $\xi_1 \leq 1.0$ and $\xi_{10} \leq 3.0$ at the inlet and outlet. For the calculation and verification, a numerical approach it can be used. To ensure a simulation with accurate boundary conditions, the Computational Fluid Dynamics (CFD) can be used as one possible method. Figure 9 shows the simulation performed in FLOTTRAN.

The total drag of the cavity of the convective air flow is shown in Eq. 6:

$$v_{am} = \sqrt{\frac{g \cdot H \cdot \Delta\theta_{am}}{Z \cdot \theta_{am,T}}}, \quad (6)$$

where $\Delta\theta_{am}$ is the increase in temperature in the cavity [K], g is the gravitational acceleration [9.81 m/s²],

$$\Delta\theta_{am} = \theta_{a,OUTLET} - \theta_{ae}, \quad (7)$$

where $\Delta\theta_{am,T}$ is the temperature at the point in the centre of mass $A = f(H, \Delta\theta_{am})$ [°C]:

$$\theta_{am,T} = \theta_{ae} + \frac{\theta_{a,OUTLET} - \theta_{ae}}{3}. \quad (8)$$

From the velocity of the convective air flow v_{am} [m/s] and cross-section of the cavity of the double-skin façade $A = L \cdot b$ [m²], the flow rate in the cavity

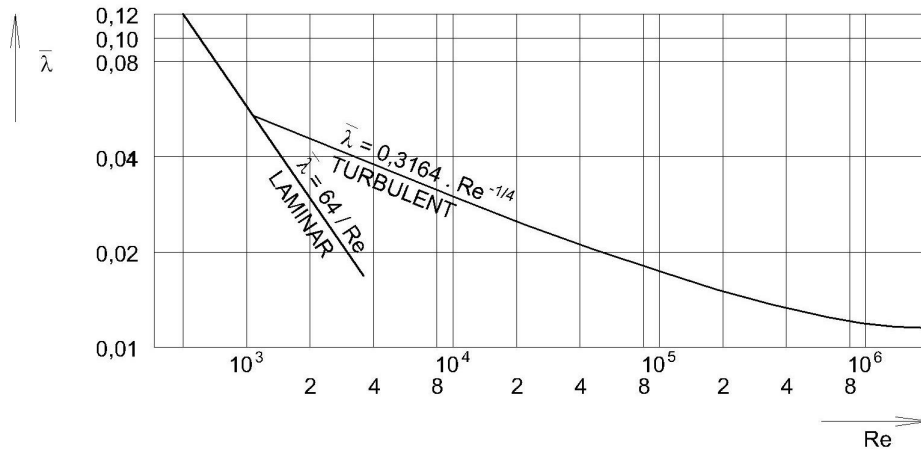


FIGURE 3. Coefficient of friction as a function of Re number.

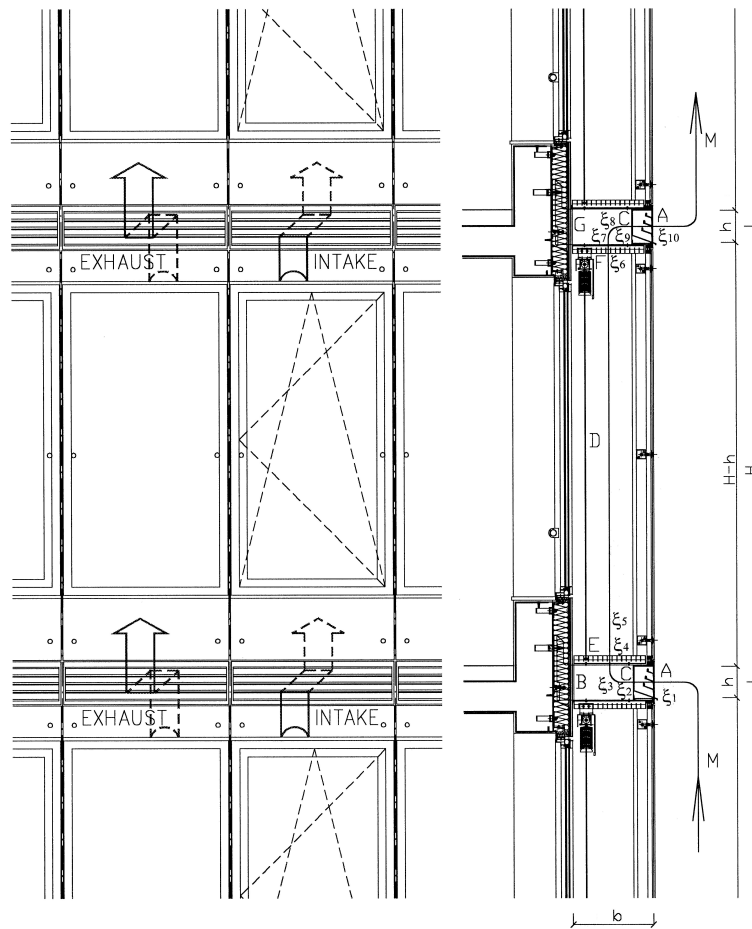


FIGURE 4. Description and quantification of aerodynamic resistances.

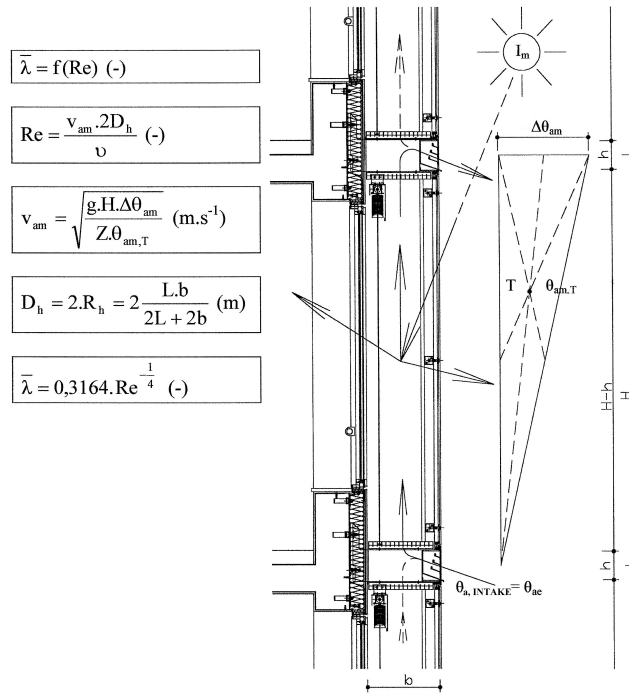


FIGURE 5. Friction resistance along the height of the convective air flow (Re – Reynolds number [-], v_{am} – air flow velocity in the cavity [m/s], ν – coefficient of kinematic viscosity of air [m²/s], g – gravitational acceleration coefficient [9.81 m/s²], θ_{am} – increase in temperature in the cavity [K], $\theta_{am,T}$ – temperature in the centre of mass $A = f(H, \Delta\theta_{am})$ [°C]).

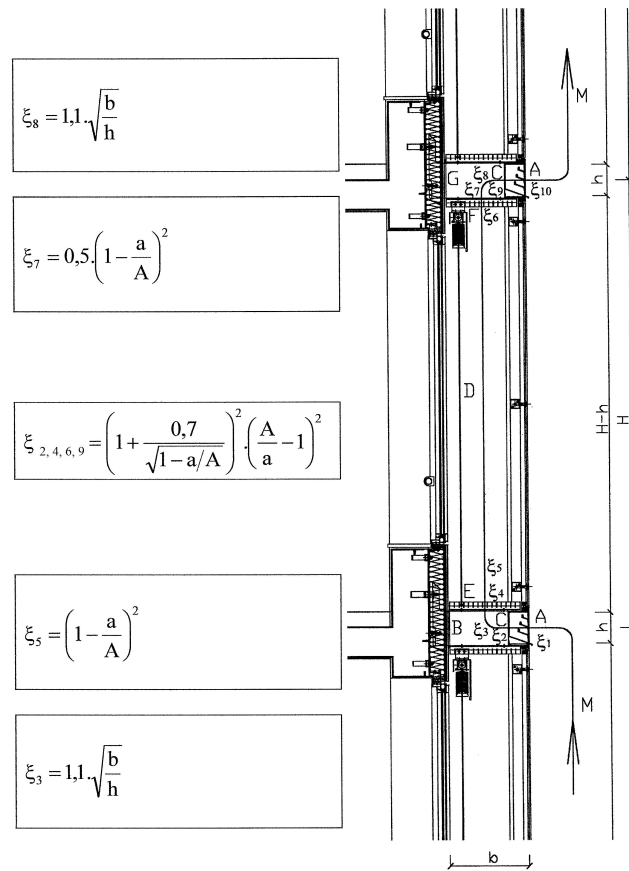


FIGURE 6. Coefficients of local resistances $\xi_2, \xi_3, \xi_4, \xi_5, \xi_6, \xi_7, \xi_8, \xi_9$ [-] in the air flow movement (a – net area opening for air movement, A – total area of the air inlet including its solid parts, b – planar width of the rectangular cross-section, h – height of rectangular cross section).

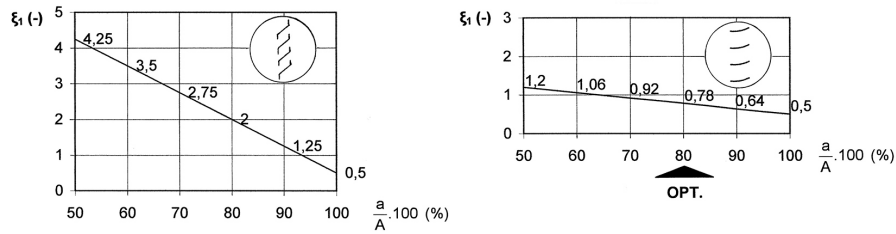


FIGURE 7. The local drag of the air flow at the inlet. Left picture illustrates the conventional rain louvers, Right picture shows aerodynamic louvers (A – total area of the inlet air, including the louvers, a – net opening area for air flow).

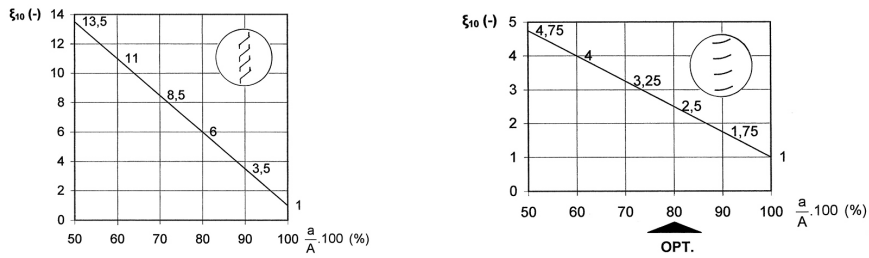


FIGURE 8. The local drag of the air flow at the outlet. Left picture shows conventional rain louvers, Right picture illustrates aerodynamic louvers (A – total area of the inlet air, including the louvers, a – net opening area for air flow).

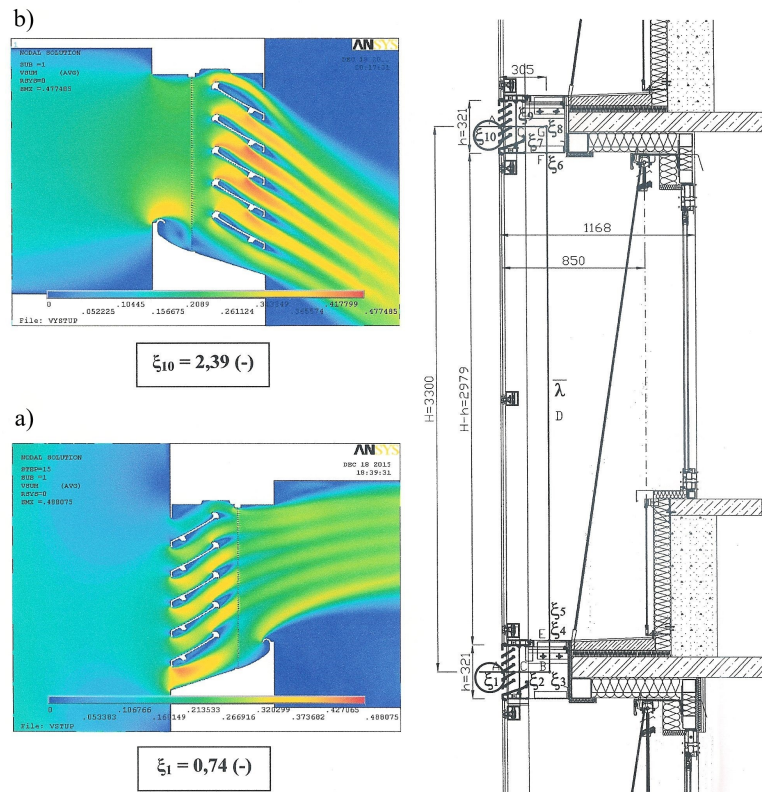


FIGURE 9. Simulation of the local aerodynamic drag coefficients ξ_1 and ξ_{10} in ANSYS FLOTTRAN. Velocity contour plot at the inlet [20].

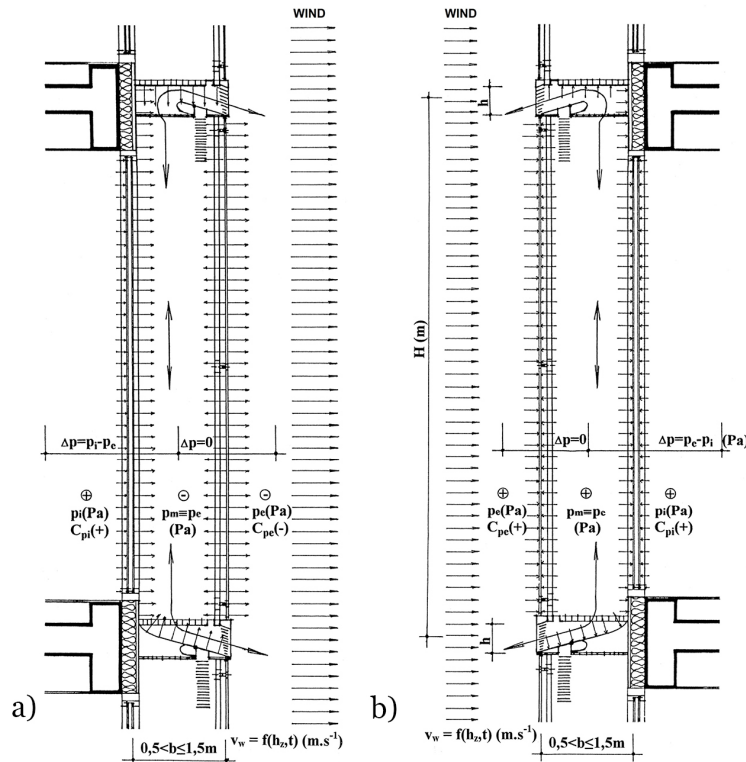


FIGURE 10. Aerodynamic loads on the DSTF with open circuit under wind condition a) Leeward side of the building, b) Windward side of the building.

can be quantified:

$$q_V = A \cdot v_{am} = L \cdot b \cdot v_{am}, \tag{9}$$

$$q_m = q_V \cdot \rho_{am,T} = L \cdot b \cdot v_{am} \cdot \rho_{am,T}, \tag{10}$$

where $\rho_{am,T}$ is the air density in the centre of mass „C“ at the temperature $\theta_{am,T}$ [kg/m³] in Figure 2.

The main requirement of the air flow in the cavity of DSTF in windless climate conditions is that Z [-] must be less than the force of the convective air buoyancy [6]. Natural convection is a phenomenon, which describes the dynamics of fluid (air) and depends on the difference of the temperature and density as a consequence of gravitational forces.

3.2. AERODYNAMIC QUANTIFICATION OF THE BUILDING – EXTERNAL PRESSURE COEFFICIENT

The external pressure coefficient has to be known to determine the airflow rate in the cavity q_m [kg/s] for wind conditions (Fig. 10):

$$c_{pe} = \frac{p - p_0}{\frac{1}{2} \rho_0 \cdot v_{w,0}^2}, \tag{11}$$

The total pressure is defined as:

$$c_p = c_p + c_{pm}, \tag{12}$$

where c_{pm} is the cavity pressure coefficient [-].

Air flow rate is defined as:

$$q_V = 2(L \cdot h) \cdot \sqrt{c_p \frac{v_{w,z}^2 \cdot \rho_{ae}}{2}}, \tag{13}$$

where $v_{w,z}$ is the gust velocity of wind [m/s], and ρ_{ae} is the density of the external air [kg/m³].

Wind loads on buildings can be evaluated from codes [21], wind tunnel tests, CFD and in-situ measurements. The data contained in standards are issued from wind tunnel experiments, performed on an isolated building in open exposure. Measurements by several works have shown that wind loads on buildings in close vicinity are considerably different from those on an isolated building. These effects arise because of the modifications of the flow field due to the surroundings. The experimental determination of the pressure coefficients is a typical aerodynamic task. It is solved on a „rigid model“ in a wind tunnel. Boundary layer wind tunnel (BLWT) is an experimental facility used for modelling the Earth’s atmosphere and it allows the experimental measurement of static and dynamic effects of wind on scale models – Figure 11. Wind tunnels with a developed atmospheric boundary layer provide a complete statistical description of the load test objects in a wind flow with a natural structure. For acquisition of external pressures from the measurement, a pressure transducer, which is conducted with plastic tubes and pressure taps with the rigid model, is used. The transducer records differential pressure. Then, according to Eq. 11, the differential pressure is divided by dynamic pressure. It is the principle of experimental measurement with a pressure transducer.

The simulated boundary layer requires similarity criteria in four basic parameters:

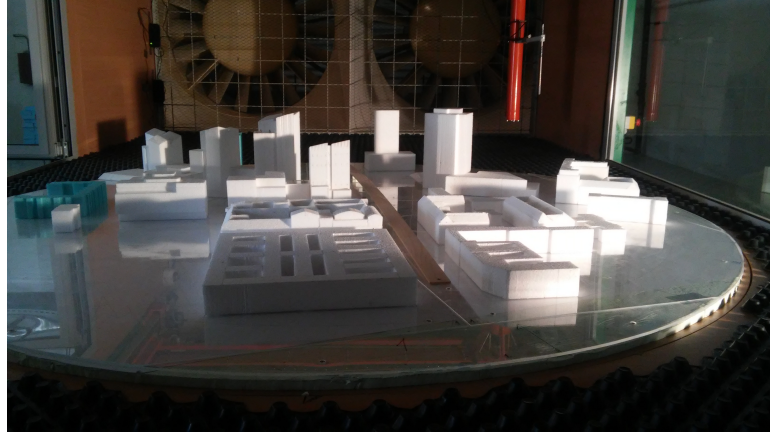


FIGURE 11. View of the measured buildings in the BLWT in Bratislava [22].

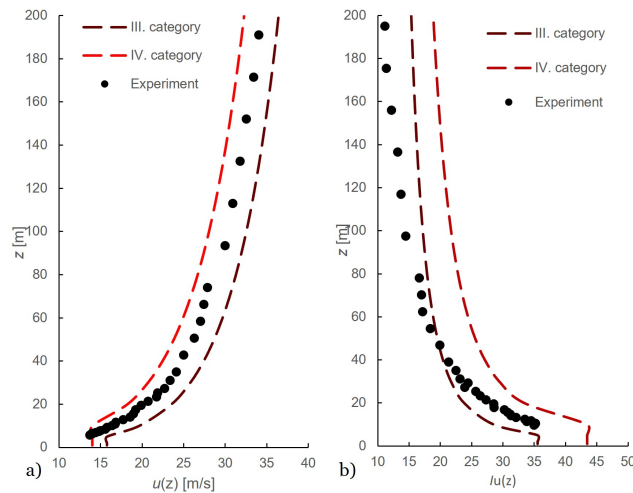


FIGURE 12. Properties of ABL in BLWT Bratislava: a) Mean wind velocity, b) Intensity of turbulence profile [23].

- (1.) longitudinal mean velocity profile,
- (2.) longitudinal turbulence intensity profile,
- (3.) turbulence integral length scale,
- (4.) non-dimensional power spectral density function.

Longitudinal mean wind velocity follows the logarithmic law according to Eq. 14. The longitudinal turbulence intensity is found to agree well with Eq. 15. The illustrative profile of mean wind velocity and turbulence intensity is in Figure 12.

$$U_{(z)} = \frac{u^*}{\kappa} \ln \frac{z}{z_0}, \quad (14)$$

$$I_u = \frac{\sqrt{u'^2}}{U_z}, \quad (15)$$

where $U_{(z)}$ is the mean wind velocity at the height z [m/s], u^* is the shear velocity [m/s], z_0 is the roughness length [m], I_u is the longitudinal turbulence intensity [-], $\sqrt{u'^2}$ is RMS of the turbulent velocity fluctuations [m/s]. Non-dimensional power spectral density is illustrated in Figure 13.

The second possible way to quantify the aerodynamic coefficients of the external pressure on the

surface of a building envelope is a simulation using Computational Fluid Dynamics (CFD). CFD is a fluid mechanics division that uses numerical analyses and algorithms to solve problems including fluid flow, heat and mass transfer and other related phenomena. There are some mathematical evaluations of an atmospheric flow simulation [25], [26]. For a simulation of convection, Navier-Stokes equations are used. The flow is treated as incompressible because the Mach number for our tasks is below 0.3. The Navier-Stokes equations for incompressible flow can be written as:

$$\frac{\partial p}{\partial t} + \frac{\partial}{\partial x_i} (\rho \bar{u}_i) = 0, \quad (16)$$

$$\frac{\partial}{\partial t} (\rho \bar{u}_i) + \frac{\partial}{\partial x_j} (\rho \bar{u}_i \bar{u}_j) = \frac{\partial}{\partial x_j} (\sigma_{ij}) - \frac{\partial \bar{p}}{\partial x_i} - \frac{\partial \tau_{ij}}{\partial x_j}, \quad (17)$$

where p is the pressure of the flow [Pa], t is the time duration [s], x is the dimension [s], u is the velocity of flow [m/s], ρ is the density of flow [kg/m³], σ_{ij} is the stress tensor [-], τ_{ij} is the subgrid-scale stress [-].

In general, there are four methods for solving N-S equations. First one is the Direct Numerical Simulation (DNS), when a problem in space and time is

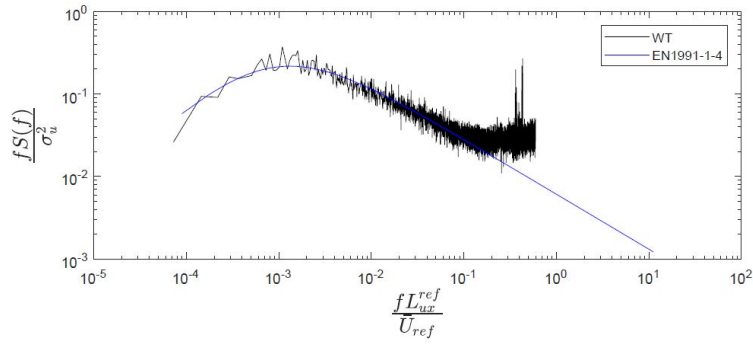


FIGURE 13. Power spectral density in BLWT Bratislava [23].

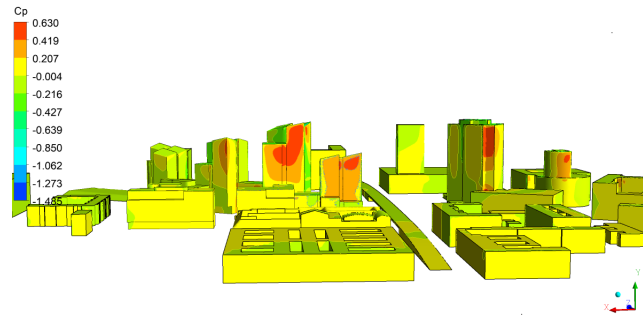


FIGURE 14. Distribution of external pressure coefficient on the envelopes of a group of buildings received from the ANSYS Fluent [22].

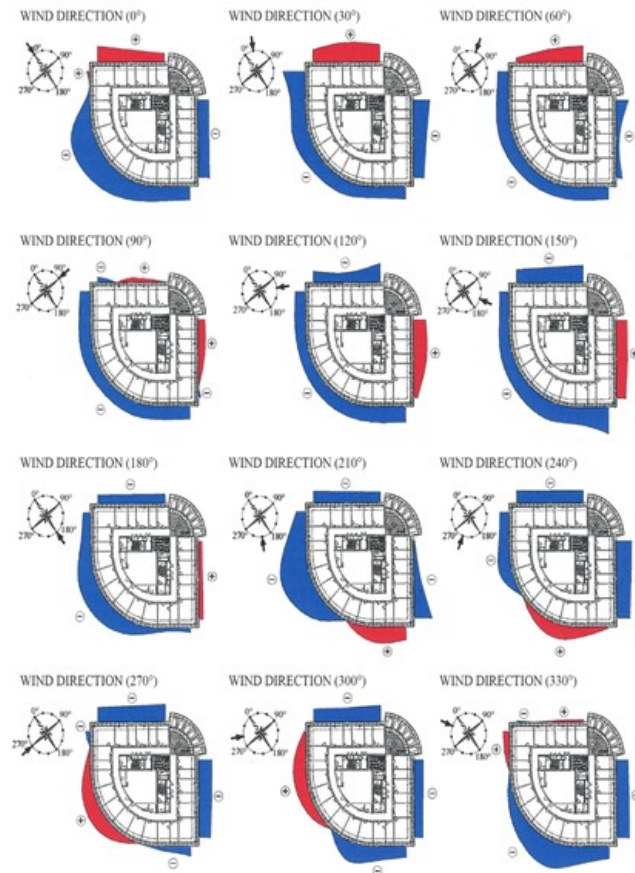


FIGURE 15. Distribution of external pressures of the building of the National Bank of Slovakia (NBS) in Bratislava on the 17th floor, $H = 56.3$ m [24].

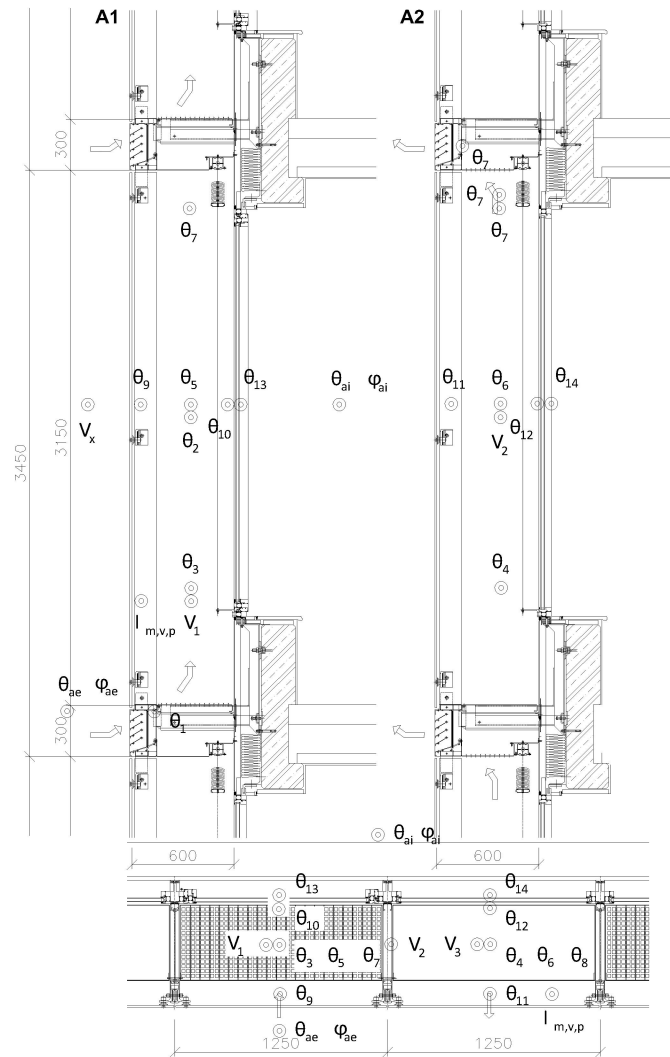


FIGURE 16. Geometry of DSTF and drawing of measured points.

solved, the second one are Reynolds Averaged N-S equations (RANS). The third method is a combination of both previous methods, which simulates large vortices and models small structures with the help of Reynolds equations. It is called the Large Eddy Simulation (LES). Current methods for solving RANS are Scale-Resolving Simulation models (SRS). An example of a graphical output of a quantification of external pressures on a building façade from the CFD calculation program is documented in Figure 14.

To obtain the overall aerodynamic pressure coefficient, it is necessary to evaluate the pressure over the entire height of a building, which is documented in Figure 15. The CFD model has to be correctly validated with experimental or situ measurements to achieve correct results. The validation procedure involves an exact modelling of the boundary conditions with experimental or situ measurements. The results are then statistically evaluated to see if they correlate with the experiment. Deviations from the experiment

are then assessed, and a numerical model is calibrated to achieve the most accurate results.

4. IN SITU

MEASUREMENT-PREPARATION

An in-situ measurement experimentally confirmed the above theory on a double-skin facade with a corridor-type cavity width = 600 mm, with an effective height of the cavity identical to the height of the floor = 3450 mm, Fig. 16. The total aerodynamic resistance of the facade was evaluated according to Eq. 3

$$\max Z = 1 + 0.20 + 14.94 = 16.14 < 18,$$

which expresses the convective buoyancy of the air. It can be stated that in terms of functional aerodynamics of the cavity, the airflow through the cavity is ensured in any climatic situation. The measuring setup monitored the temperature and aerodynamic regimes of DSTF during 18 months on the 17th floor of a southwest façade, which was 56.3 m in height. The

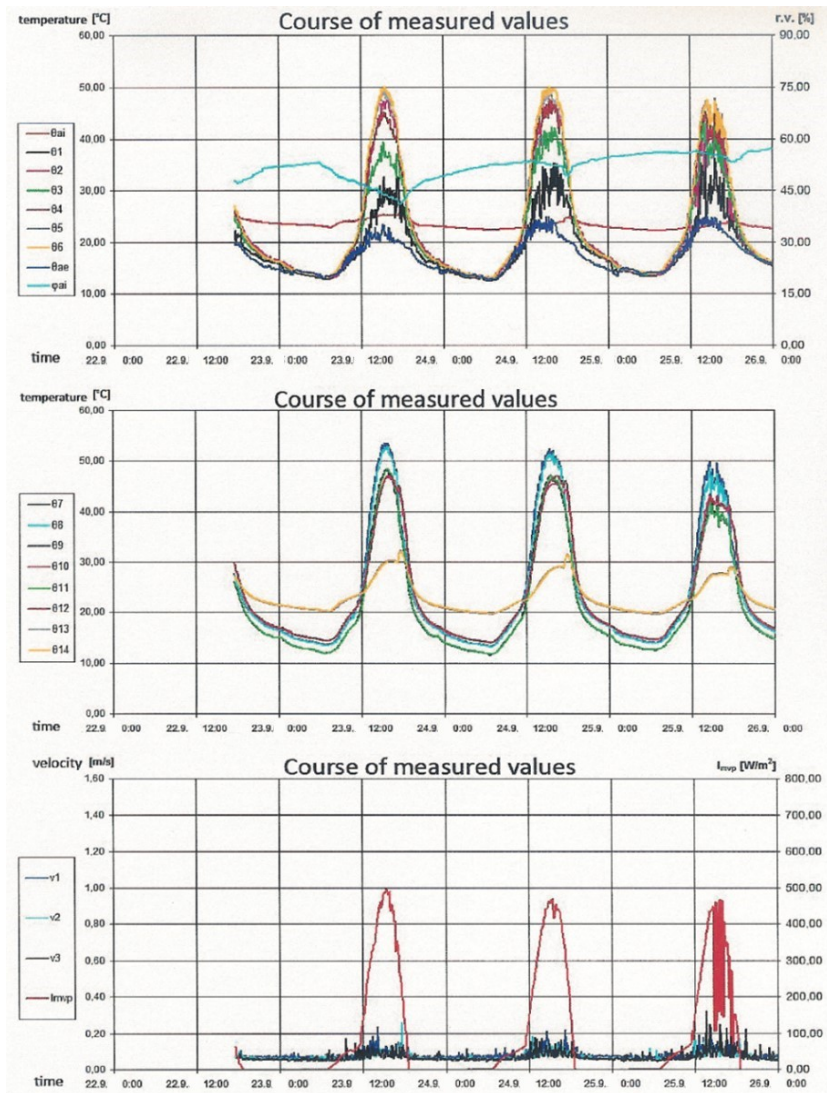


FIGURE 17. Measured variables from the experiment for the typical period of clear windless warm weather.

recorded parameters were the temperature, relative humidity, and wind velocities in the control points, as is shown in Fig. 16.

Due to the large volume of measuring points and results, we will focus on the critical state of windless conditions in this article. When the airflow in the cavity of DSTF is based on natural convection. Recording of the measured variables in the cavity for the period of clear windless warm weather is illustrated in Fig. 17.

5. RESULTS AND DISCUSSION

The following conclusions were found based on long-term measurements of temperatures, the effects of solar radiation and relative humidity in-situ conditions when the facade was treated under windless conditions, Fig. 18:

- the convection occurs in the cavity at every time step with the velocity ranging from $0.05 \leq v \text{ [m/s]} \leq 0.2$ to 0.3 ,
- the convective velocity through the cavity increases due to the growth of global solar radiation,

- the energy regime in the cavity is characterised by inhomogeneity due to the alternating position of the air inlet and air outlet modules,
- in the cavity, there are 3 characteristic zones for aerodynamic and thermal regimes:
 - zone of increasing temperatures (around 29°C) along the height of the cavity in the inlet – the movement of convective airflow,
 - a large area with temperatures in the air outlet-stagnation of air (around 47°C)
 - a small area with particularly high temperatures in the upper part of the inlet (around 53°C) – the state of no flow, stagnation of air. This means a 29°C temperature gradient as compared to the outside temperature.

Based on these results, we can evaluate a constant airflow in any climatic situation, even in windless conditions. It confirms the correct physical function of the cavity and testifies to the quality of DSTF in terms of its aerodynamic dimensions.

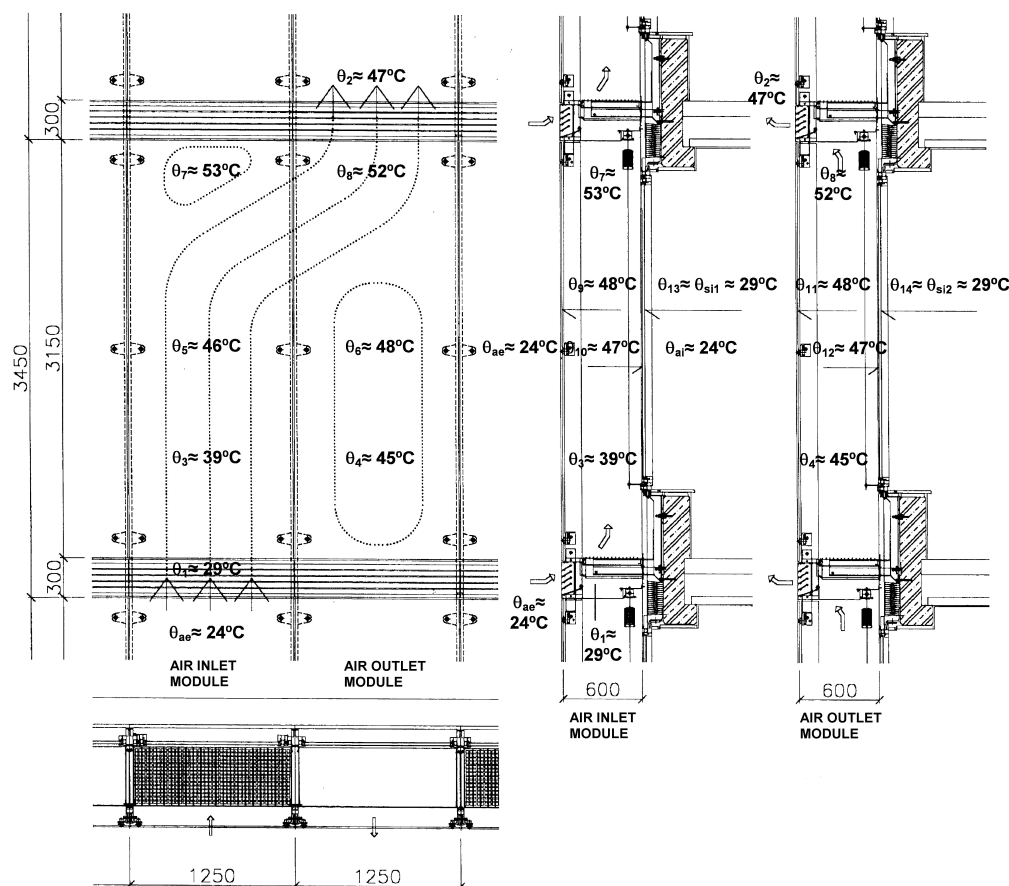


FIGURE 18. The resulting temperature zones during the clear windless warm weather.

6. CONCLUSIONS

The theory and practice of natural physical cavities is a very significant area of the future façade technologies of intelligent buildings. It is directly connected with two very efficient and available alternative energy sources, solar radiation and wind energy, but most often, their very significant combinations. Natural physical cavities allow for wide modifications in the creation of the new façade technology of buildings in the material-structural and shape-aesthetic concepts of modern architecture.

The functional aerodynamics of the cavity of the DSTF in any climatic situation (even in a critical windless state) is an essential precondition for its optimal temperature and energy regime. It can be seen from the experience of the implementation of naturally ventilated DSTF in the modern world that underestimating the dimensioning of elements can lead to severe defects. It can lead to an uncomfortable temperature regime (stagnation of hot air in the cavity in summer). To quantify the temperature and energy regime of DSTF, we must know two basic aerodynamic inputs:

(1.) aerodynamic quantification of the building characterised by an external pressure coefficient, which we can obtain from experimental measurements in the BLWT or from CFD simulations,

(2.) aerodynamic quantification of the interspace characterised by its total aerodynamic resistance.

With their help, we can quantify the air flow through the cavity, the increase in temperature and the resulting energy efficiency of the façade. In-situ measurements of the temperature, aerodynamic, and energy regime of the DSTF during its operation can serve as a standard for debugging and refining calculation procedures and simulation programs. These results significantly contribute to the development of the science and practice.

The design of DSTF has to integrate the multidiscipline approach to ensure the low energy needs. Only a global view can provide a development in the field of architecture.

ACKNOWLEDGEMENTS

This work was supported by the Scientific Grant Agency MŠVVŠ SR and SAV under VEGA 1/0113/19, Slovak Research and Development Agency under the contract No. APVV-21-0144.

REFERENCES

- [1] B. Bielek, J. Híreš, D. Lukášik, M. Bielek. *Development of technology in architecture for sustainable society*. Nakladateľstvo STU, Bratislava, 2012.
- [2] B. Todorovic, B. Maric. *The influence of double facades on building heat losses and cooling loads*.

- Faculty of Mechanical Engineering, Belgrade University, Belgrade, Yugoslavia, 1999.
- [3] D. M. Arons. *Properties and applications of double-skin building facades*. Ph.D. thesis, Massachusetts Institute of Technology, 2000. <http://hdl.handle.net/1721.1/8724>.
- [4] G. Gan. Thermal transmittance of multiple glazing: computational fluid dynamics prediction. *Applied Thermal Engineering* **21**(15):1583–1592, 2001. [https://doi.org/10.1016/S1359-4311\(01\)00016-3](https://doi.org/10.1016/S1359-4311(01)00016-3).
- [5] D. Saelens, H. Hens. Experimental evaluation of airflow in naturally ventilated active envelopes. *Journal of Thermal Envelope and Building Science* **25**(2):101–127, 2001. <https://doi.org/10.1106/CU0X-XL16-6QTA-29QC>.
- [6] J. Hensen, M. Bartak, F. Drkal. Modeling and simulation of a double-skin façade system. *ASHRAE Transactions* **108**(2):1251–1259, 2002.
- [7] D. Saelens. *Energy performance assessment of single storey multiple-skin facades*. Ph.D. thesis, Katholieke Universiteit Leuven, Belgium, 2002.
- [8] E. Gratia, A. De Herde. Natural ventilation in a double-skin facade. *Energy and Buildings* **36**(2):137–146, 2004. <https://doi.org/10.1016/j.enbuild.2003.10.008>.
- [9] J. von Grabe. A prediction tool for the temperature field of double facades. *Energy and Buildings* **34**(9):891–899, 2002. [https://doi.org/10.1016/S0378-7788\(02\)00065-8](https://doi.org/10.1016/S0378-7788(02)00065-8).
- [10] N. Mingotti, T. Chenvidyakarn, A. W. Woods. The fluid mechanics of the natural ventilation of a narrow-cavity double-skin facade. *Building and Environment* **46**(4):807–823, 2011. <https://doi.org/10.1016/j.buildenv.2010.09.015>.
- [11] K. Nore, B. Blocken, J. Thue. On CFD simulation of wind-induced airflow in narrow ventilated facade cavities: Coupled and decoupled simulations and modelling limitations. *Building and Environment* **45**(8):1834–1846, 2010. <https://doi.org/10.1016/j.buildenv.2010.02.014>.
- [12] J. M. Blanco, P. Arriaga, E. Rojí, J. Cuadrado. Investigating the thermal behavior of double-skin perforated sheet façades: Part A: Model characterization and validation procedure. *Building and Environment* **82**:50–62, 2014. <https://doi.org/10.1016/j.buildenv.2014.08.007>.
- [13] H. Manz, H. Simmler. Experimental and numerical study of a mechanically ventilated glass double façade with integrated shading device. In *Research in Building Physics*, pp. 519–526. CRC Press, 2020. <https://doi.org/10.1201/9781003078852-71>.
- [14] Z. Zeng, X. Li, C. Li, Y. Zhu. Modeling ventilation in naturally ventilated double-skin façade with a venetian blind. *Building and Environment* **57**:1–6, 2012. <https://doi.org/10.1016/j.buildenv.2012.04.007>.
- [15] J. Parra, A. Guardo, E. Egusquiza, P. Alavedra. Thermal performance of ventilated double skin façades with venetian blinds. *Energies* **8**(6):4882–4898, 2015. <https://doi.org/10.3390/en8064882>.
- [16] W. Streicher, R. Heimrath, H. Hengsberger, et al. On the typology, costs, energy performance, environmental quality and operational characteristics of double skin façades in european buildings. *Advances in Building Energy Research* **1**(1):1–28, 2007. <https://doi.org/10.1080/17512549.2007.9687267>.
- [17] B. Bielek, M. Bielek, M. Palko. *Double-skin transparent facades of buildings*. Coreal, Bratislava, 2002.
- [18] A. Compagno. *Intelligent glass facades: material, practice, design*. Birkhauser, 1995.
- [19] E. Oesterle. *Double skin facades: integrated planning; building physics, construction, aerophysics, air-conditioning, economic viability*. Prestel, 2001.
- [20] M. Palko, A. Palková. Selected aerodynamic problems of double skin facade. *Advanced Materials Research* **1057**:137–144, 2014. <https://doi.org/10.4028/www.scientific.net/AMR.1057.137>.
- [21] STN EN 1991-1-4. Eurocode 1: Actions on structures. Part 1-4: General actions. Wind actions. Slovak Office of Standards, Metrology And Testing, 2007.
- [22] O. Hubová, M. Macák, M. Franek, V. Mitro. *CFD Simulation and Experimental Verification of Wind Flow around Building Complex in Budapest*. Slovak University of Technology, 2017.
- [23] M. Franek. *Impact of the interference effects on the distribution of the external pressure coefficient for elliptic high – rise buildings*. Ph.D. thesis, Slovak University of Technology, 2017.
- [24] L. Ilg, B. Bauhofer. *Slowakische Nationalbank Zentrale in Bratislava – Windrück an der Gebäudekülle – Windkanalstudie*. ETH Zürich – HL-Technik AG München, 1996.
- [25] D. C. Wilcox, et al. *Turbulence modeling for CFD*, vol. 2. DCW industries La Canada, CA, 1998.
- [26] K. Hanjalić, B. Launder. *Modelling turbulence in engineering and the environment: second-moment routes to closure*. Cambridge University Press, 2011.